Cloud Effects in Hyperspectral Imagery from First-Principles Scene Simulations

S.M. Adler-Golden[*a], D.C. Robertson[a], S.C. Richtsmeier[a] and A.J. Ratkowski[b]
[a]Spectral Sciences, Inc., 4 Fourth Avenue, Burlington, MA 01803-3304
[b]Air Force Research Laboratory, 29 Randolph Road, Hanscom AFB, MA, 01731-3010

ABSTRACT

Clouds and cloud fields introduce important backscattering, obscuration, shadowing and radiative trapping effects in visible-NIR(near-infrared)–SWIR(short-wavelength infrared) hyperspectral imagery of the ground, especially in off-nadir (slant) viewing geometries where cloud thickness effects reduce the cloud-free line of sight (CFLOS). An investigation of these effects was conducted using monochromatic, multispectral and hyperspectral scene simulations performed with the Spectral Sciences, Inc. MCScene Monte Carlo code. Cloud fields were obtained from the Cloud Scene Simulation Model (CSSM) of Cianciolo and Raffensberger. The simulations took advantage of a data-fusion-based noise-removal method that enabled a dramatic reduction in computation time. Illumination levels at the sunlit ground showed enhancements of up to ~50% due to cloud scattering. Illumination in the cloud shadows was 20% of the full solar illumination or greater, with cloud optical depths of up to 10. Most of this illumination arises from solar scattering off the cloud tops and sides; however, a significant part can be ascribed to radiative trapping between the ground and the clouds, as represented by a local atmospheric spherical albedo. A simulation of a hyperspectral scene with cloud shadows was found to reproduce shadowing effects found in real data. Deeper shadowing is observed with increasing wavelength and in water-band regions, consistent with a previous analysis of cloud shadows in real imagery. The MCScene calculations also predict shadow enhancements of column water vapor retrievals from atmospheric correction/compensation codes, also in accord with field observations. CFLOS fractions were calculated as a function of off-nadir viewing angle and were found to be very accurately represented by a semi-empirical analytical function of both angle and cloud cover.

Keywords: hyperspectral, scene, cloud, simulation, CFLOS, multispectral

INTRODUCTION

Clouds and cloud fields considerably complicate the analysis of visible-NIR-SWIR hyperspectral and multispectral imagery. In addition to obscuring the ground, clouds introduce important shadowing and radiative trapping effects. In this paper, model-based comparisons are used to illustrate and characterize cloud field impacts from the standpoint of spectral image analysis, including atmospheric correction or compensation, and focusing on off-nadir (slant) viewing geometries, where the cloud-free line of sight (CFLOS) fraction is generally smaller than in nadir views.

Increased obstruction of the LOS by clouds at large off-nadir viewing angles is a limiting factor in the utility of slant viewing geometries. This is illustrated by a recent analysis of two highly off-nadir (8º at the ground) hyperspectral images taken by NASA's Hyperion sensor.[1] In these images, taken in opposite directions along the flight path, large fractions of the ground were obstructed by clouds and contaminated by cloud shadows, despite reports of low cloud cover over the target area. In general, ground views at a given cloud cover fraction, which we denote f_0, become increasingly obstructed as the off-nadir angle is increased due to the finite thickness of the cloud.[2,3] Therefore cloud cover considered acceptable for nadir viewing may prove to be unacceptable for highly off-nadir viewing.

Another critical cloud effect is shadowing. Retrieval of surface reflectance spectra from the radiance data, known as atmospheric correction or compensation, requires accurate removal of the path radiance (atmospheric scattering) contribution. In cloud shadows the retrieved reflectance is greatly reduced, making its spectral shape proportionally more sensitive to any error in the path radiance estimate. This sensitivity increases further at large off-nadir viewing angles due to the increased atmospheric path. Further spectral shape distortion in cloud shadows can arise from wavelength-dependent cloud optical properties.

[*]adlergolden@spectral.com; phone 781 273-4770; fax 781 270-1161; spectral.com

In a continuing effort to quantify off-nadir viewing effects in spectral imagery, we have performed a series of cloudy scene simulations with our MCScene first-principles Monte Carlo radiation transport code.[4,5] MCScene incorporates a cloud overlay from the semi-empirical Cloud Scene Simulation Model (CSSM) of Cianciolo and Raffensberger,[6] which uses stochastic field generation techniques and convection physics to generate realistic three-dimensional (3-D) distributions of water particulates and vapor. CSSM cloud fields generated for three cloud types, nimbostratus, stratocumulus and cumulus, were used in monochromatic MCScene simulations with a uniform surface reflectance. The results led to a quantitative description of cloud obscuration and shadowing as a function of viewing and solar angles, and also provided insights into cloud shadowing and illumination effects for both nadir- and slant-viewing imagery. In addition, an off-nadir hyperspectral image of a rural scene with 121 spectral channels and an overlaid nimbostratus cloud field was simulated using MCScene. A data fusion technique described in the Appendix to this paper, which provides substantial noise reduction, was employed to yield a high-fidelity output with 200 Monte Carlo "photons" per pixel per spectral channel. This calculation ran overnight on a Beowulf PC cluster with 40 processes. The simulated hyperspectral data cube was atmospherically corrected using the first-principles FLAASH algorithm[7,8] and was compared with the input surface reflectance data to provide a consistency check on FLAASH and MCScene.

Simulation approach

The Monte Carlo Scene code (MCScene), described elsewhere[4,5], is a first-principles, high-fidelity HSI/MSI image simulation algorithm based on a Direct Simulation Monte Carlo (DSMC) approach for modeling 3-D radiation transport. With this approach, "ground truth" is accurately known through input specification of surface and atmospheric properties. The well-known drawback to the DSMC approach is the large number of trial "photons" needed to achieve an accurate result, leading to long computation times. However, recent advances in computing speed combined with parallel processing are mitigating this limitation.

MCScene incorporates all optical effects important for solar-illuminated scenes, including molecular and aerosol scattering and absorption, scattering events, surface scattering with material-dependent bidirectional reflectances, multiple surface adjacency effects, scattering and shading by clouds, and arbitrary solar illumination and sensor viewing geometries. As shown in Fig. 1, the calculation region is a cube, nominally 50 km on a side, enclosing a base representing the ground and a user-definable atmosphere containing molecular species, aerosols and clouds. The sensor spatial and spectral resolution, location and viewing angle are also specified. A finely gridded inner calculation region occupying the sensor's field of view (FOV) contains spatially varying surface elevations, reflectances and atmospheric properties. Realistic spectral-spatial statistics may be obtained by using surface reflectance properties derived from atmospherically corrected hyperspectral data. The region outside the FOV contributes to adjacency effects, that is, the effects of photons that reflect off the ground elsewhere and then scatter into the FOV.[9] This outside region is treated as horizontally homogeneous, a simplification that should affect only the edges of the FOV, since the length scale of adjacency scattering typically is on the order of hundreds of meters. The reflectance functions for ground materials are specified as either Lambertian or via a modified version of a Walthall surface bidirectional reflectance model.[10]

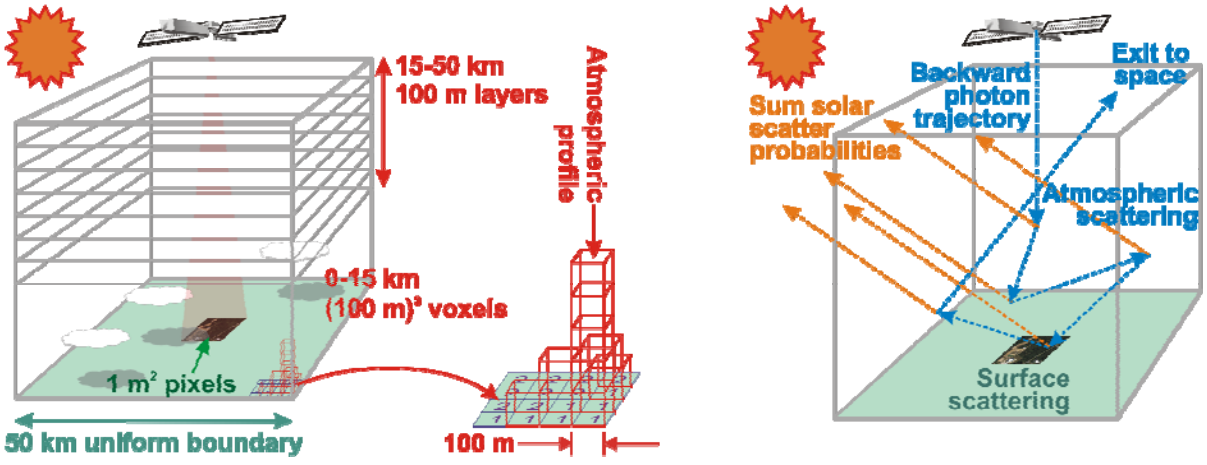

Fig. 1. Elements of the scene definition in the MCScene model (left) and illustration of the backward DSMC approach used to track trial photons (right).

In MCScene's backward DSMC method, photons are launched from the sensor toward the ground, their trajectories are followed, and their contributions to the apparent reflectance are accumulated as a function of pixel position to build up the scene at a given wavelength. Along these trajectories, the photons may be scattered by molecules, aerosols or clouds, they may be absorbed, or they may reflect off the ground or an object. A given photon may undergo multiple scattering events. Optical property databases from MODTRAN®[11] provide the required spectral scattering and absorption data for MCScene. Considerable effort has been expended to optimize the computational efficiency of the code. Since every photon trajectory at every wavelength is calculated independently of every other, parallel computing on a Beowulf cluster yields dramatic speed improvements.

To generate cloudy MCScene images, realistic three-dimensional cloud optical depth distributions were calculated with the Cloud Scene Simulation Model (CSSM) of Cianciolo and Raffensberger[6] for cirrocumulus, cirrus, nimbostratus and stratocumulus cloud types. The cloud fields span an area of 15 km x 15 km with volumetric resolution elements (voxels) of 20 m on a side The voxel optical properties (extinction coefficient, single-scattering albedo and scattering phase function asymmetry parameter) were generated from the CSSM optical depths at 73 wavelengths from 0.4 to 2.5 μm using MODTRAN® databases.

Off-nadir viewing through cloud fields

A key quantity to be extracted from the cloud scenes is the line-of-sight (LOS) cloud fraction, denoted f, as a function of the off-nadir angle, θ and azimuth angle for a given cloud cover fraction, f_0, which corresponds to a nadir view. The quantity 1-f is referred to in the literature as the cloud-free line of sight (CFLOS). A MCScene calculation performed at a wavelength of 1.0 μm with a surface reflectance value of zero proved sufficient for determining f by simple thresholding of the pixel value (the MCScene output units are apparent reflectance). These results are insensitive to sun location, which was taken as 30º from zenith. Sensor height was set well above the clouds to mimic the parallel LOS scenario. An additional calculation performed with a higher surface reflectance value, such as 0.25, enabled partitioning of the cloud-free area and determination of the fraction of the image taken up by the cloud shadows. Shadowing significantly affects the utility of the image; moderate levels of shadow (up to ~60% illumination reduction) may be treated reasonably well with shadow removal methods or shadow-insensitive detection[12,13], while deeper shadows are more problematic.

Examples of MCScene images and a cloud and shadow classification map are shown in Fig. 2. These 512x512 pixel images were generated at 20 m pixel resolution using 1000 Monte Carlo photons per pixel and a nimbostratus cloud field with a cloud cover cloud cover fraction of 0.38. The sensor was located at 50 kft, with the center LOS at a 45º off-nadir angle and a 270º azimuth angle from due East (that is, viewing North); the sun was located at 30º zenith and 170º azimuth. The classification map at right was generated after applying a 5x5-pixel smoothing window. Maps of similar fidelity were obtained using as few as 100 Monte Carlo photons per pixel.

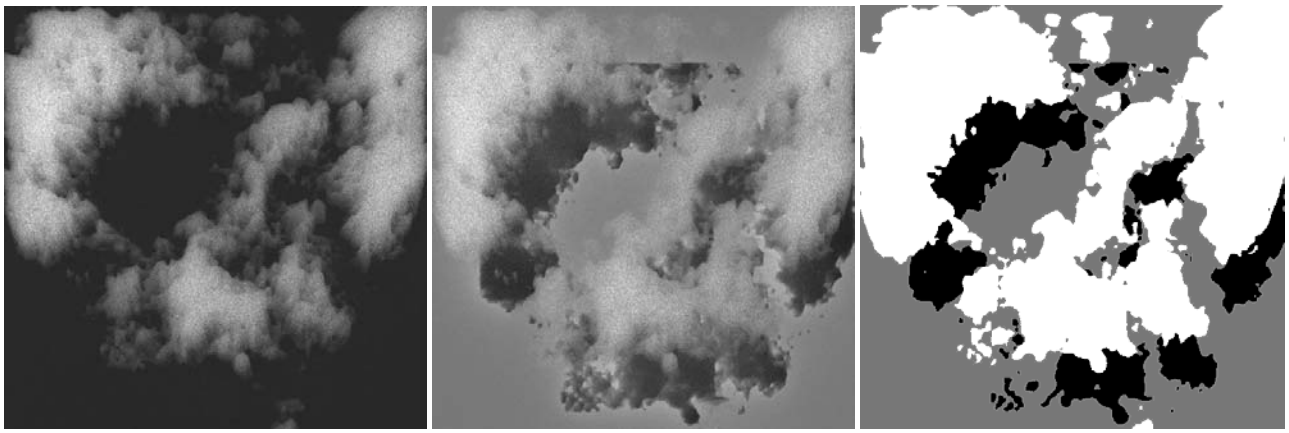

Fig. 2. MCScene images of nimbostratus clouds at a viewing angle of θ = 45º with ground reflectances of 0 and 0.25 at left and center, respectively. The classification map (white=cloud, black=shadow, gray=sunlit) is at right.

The classification map in Fig. 2 illustrates a model difficulty in calculating shadow coverage from the direct MCScene simulations: the FOV includes ground areas that lack shadow due to the finite spatial extent of the model cloud field. This effect is especially pronounced at high off-nadir angles. For example, note that in Fig. 2 the cloud field's top edge produces a horizontal shadow edge near the top of the 0.25 reflectance image. As a result, the shadow coverage is lower than what would be obtained from an extended cloud field. This problem could be remedied with a couple of different approaches. One would be to extend the cloud field via mirror reflections at the boundaries. Another approach, which may better predict average behavior, would be to estimate the shadow coverage statistically, assuming random spatial correlation between the shadows and the clouds. This should be valid as long as the sun and sensor are not closely aligned (if the sun is directly behind the observer, in the "hotspot", the shadows are obscured by the clouds). In this approach, the shadow fraction at the ground would be represented by the LOS cloud fraction at the solar zenith angle ϕ, denoted $f(\phi)$, and the net, unobscured shadow fraction in the image would be given by the product of $f(\phi)$ and the unobscured image fraction $1\text{-}f(\theta)$.

Since cloud cover varies locally, a meaningful comparison of LOS cloud fractions at different off-nadir viewing angles requires that the simulated images cover the same nominal region of the cloud field. To satisfy this condition, the image FOVs were co-aligned at the mean height of the cloud layer, as shown in Fig. 3. A pushbroom geometry input option in MCScene was used, in which the image size and location are defined by a cross-track angle and an along-track displacement along the ground, which has a simple functional dependence on the off-nadir viewing angle θ.

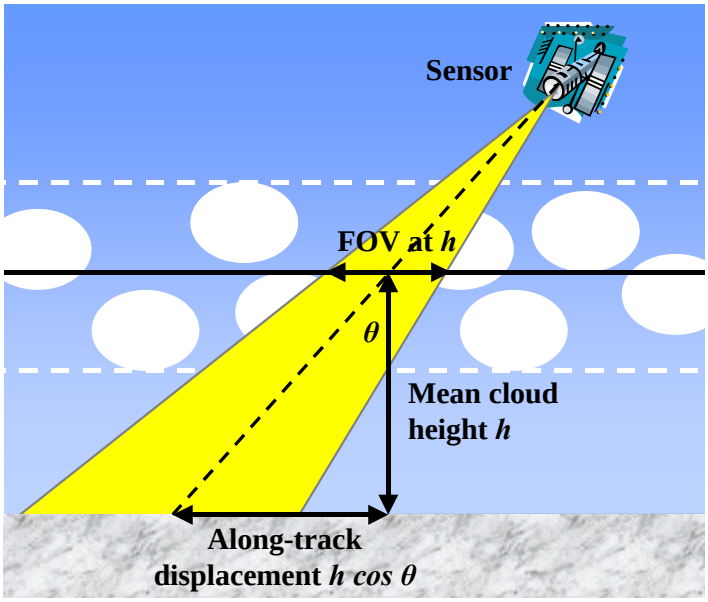

Fig. 3. Geometry for image alignment with the cloud field. Clouds are located in a horizontal layer between the dashed lines. The angle-dependent displacement along the ground provides co-alignment of the images at the mean cloud layer height.

CFLOS results

To characterize the CFLOS ($1\text{-}f$) as a function of off-nadir angle, a set of four cloud-aligned images corresponding to off-nadir angles of 0, 30, 45 and 60º were generated for each viewing azimuth angle and cloud type. The results are given in Tables 1 and 2 in terms of f, the LOS cloud fraction. As expected, the f values increase steadily with increasing off-nadir angle. The two sets of results for the same nimbostratus cloud field viewed from opposite azimuthal directions agree very closely, to within around 0.01, suggesting that the calculations provide excellent statistical sampling of the cloud field. The cirrus LOS cloud fractions were calculated for several different azimuth angles, and show a marked azimuth dependence due the strong striations in the cloud field (Fig. 4).

All of the results are in excellent agreement, to within ~0.01, with a semi-empirical analytical model, described in the next section. The off-nadir dependence of the CFLOS is described by the nadir CFLOS and a single free parameter, r, that depends on the cloud type and, for striated clouds, on the azimuth angle.

Table 1. LOS cloud fraction versus off-nadir angle θ for nimbostratus and stratocumulus clouds.

Cloud type	**Nimbostratus**	**Nimbostratus**	**Model *r* = 0.9**	**Stratocumulus**	**Model *r* = 1.4**
Azimuth =	0 º	180 º	-	270 º	-
θ = 0 º	0.376	0.374	0.374	0.379	0.379
θ = 30 º	0.423	0.412	0.410	0.466	0.458
θ = 45 º	0.483	0.467	0.468	0.568	0.559
θ = 60 º	0.567	0.554	0.580	0.717	0.713

Table 2. LOS cloud fraction versus off-nadir angle θ for cirrus clouds. Striations are oriented approximately along azimuth angle = 235º.

	225 º Azimuth	**Model *r* = 0.75**	**270 º Azimuth**	**Model *r* = 0.9**	**315 º Azimuth**	**Model *r* = 1.25**
θ = 0 º	0.313	0.313	0.332	0.332	0.312	0.312
θ = 30 º	0.325	0.336	0.365	0.365	0.372	0.369
θ = 45 º	0.376	0.375	0.418	0.419	0.463	0.450
θ = 60 º	0.442	0.460	0.513	0.526	0.585	0.590

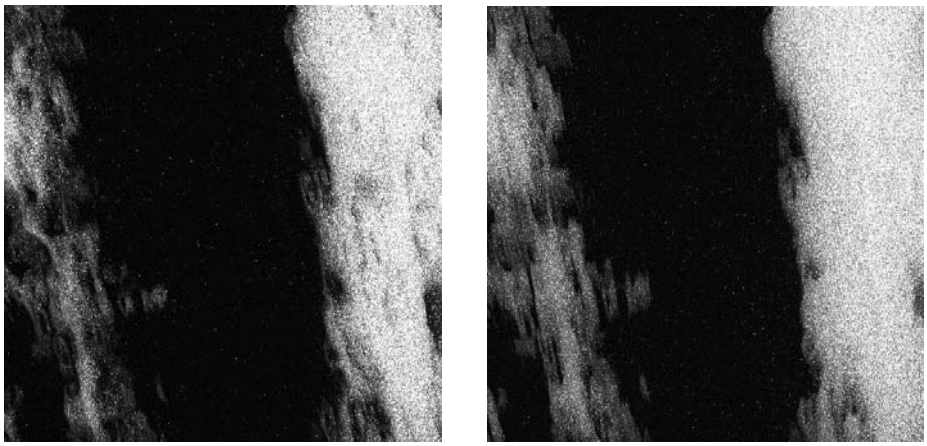

Fig. 4. Cirrus cloud field images at 225º azimuth, 0º off-nadir (left) and 60º off-nadir (right).

Analytical cloud cover model

To understand and model the MCScene CFLOS results, we have developed an analytical parameterization that accounts for the simple geometric effects of broken clouds by modeling them as ellipsoids located randomly in a uniformly thick horizontal layer, as depicted in Fig. 3. The approach is based on an analogy with Beer's law for optical absorption, where the unobscured image fraction corresponds to transmittance and the cloud cross-sectional area corresponds to a molecular absorption cross section. That is,

$$\begin{aligned} 1-f &= \exp\left(-\sigma N\right) \\ &= \exp\left(-c/\cos\theta\right) \end{aligned} \tag{1}$$

where σ is the cloud cross-sectional area and N is the cloud column density (number per unit area). In the second line of Eq. (1), the variables are factored into the angular dependence of the column density (1/cosθ) and a variable c that includes σ and the cloud layer thickness.

For spherical clouds σ, and hence c, would be independent of θ. In that case, c is given by

$$c_{spherical} = -\ln\left(1-f_0\right) \tag{2}$$

where f_0 is the (nadir-viewing) cloud cover fraction. More generally, the clouds may be modeled as oblate or prolate ellipsoids. Here the cross-sectional area and hence c scale with the projected height of the ellipsoid, given by

$$h = 2\sqrt{a^2 \sin^2\theta + b^2 \cos^2\theta} \tag{3}$$

where a and b are the ellipsoid axis lengths in respectively the vertical (z) and horizontal (x,y) directions, respectively. This leads to a generalization of Eq. (2),

$$c = -\ln(1 - f_0)\sqrt{r^2 \sin^2\theta + \cos^2\theta} \tag{4}$$

where $r = a/b$ is the effective height-to-width ratio of the ellipsoids. Note that in the flat-cloud limit (r=0) the angular dependence in Eq. (1) drops out, as expected.

As shown in Tables 1 and 2, the model provides an excellent fit to the MCScene/CSSM simulations. Azimuthally isotropic cloud fields yield similar r values in all azimuthal directions. In contrast, cloud fields that are highly striated, such as the CSSM cirrus clouds, yield azimuthally-dependent r values. This dependence might be modeled with a cloud field of scalene ellipsoids.

Ground illumination variation in cloud fields

Illumination levels under a cloud field reflect a complex phenomenology. Direct transmission of sunlight through opaque clouds is very low, except at cloud edges. However, there is substantial surface illumination in the shadows from sunlight scattered through the edges of the cloud and from neighboring clouds. The effect of edge scattering can also be significant for some surfaces that are fully sunlit. There is also some enhancement of the illumination by radiative trapping, that is, by reflection of light coming up from the ground back down toward the ground. The effective downward reflectivity for a horizontally homogeneous atmosphere is defined by an atmospheric spherical albedo, S, which appears in the standard radiation transport equation for earth surface viewing.[7] The illumination enhancement factor is given by $1/(1-\rho S)$, where ρ is a spatially averaged ground reflectance. One can generalize the definition of the spherical albedo, S, for partial cloud cover.

These illumination enhancement effects may be seen in Fig. 5 in a MCScene simulation with the nimbostratus cloud field at 45º off nadir and 0.25 ground reflectance. The minimum apparent reflectance value in the scene, corresponding to the darkest cloud shadow, is 0.06. This corresponds to an illumination fraction of 0.06/0.25 = 24%. This is near the low end of the range of cloud shadow illuminations that we have observed in measured spectral imagery of scenes with opaque clouds. Slightly lower values are found with cirrus cloud fields. Enhancement of illumination outside the shadow by cloud scattering may be seen in the profile along the dashed horizontal line. Here the apparent reflectances outside the shadow are up to 0.05, or 20%, higher than the 0.25 surface reflectance, due to the added illumination from scattering off or through nearby clouds. This scattering undoubtedly contributes to illumination in the shadow. The largest cloud scattering enhancement in the scene is 50% and occurs in a narrow break between the clouds, as indicated by the arrow.

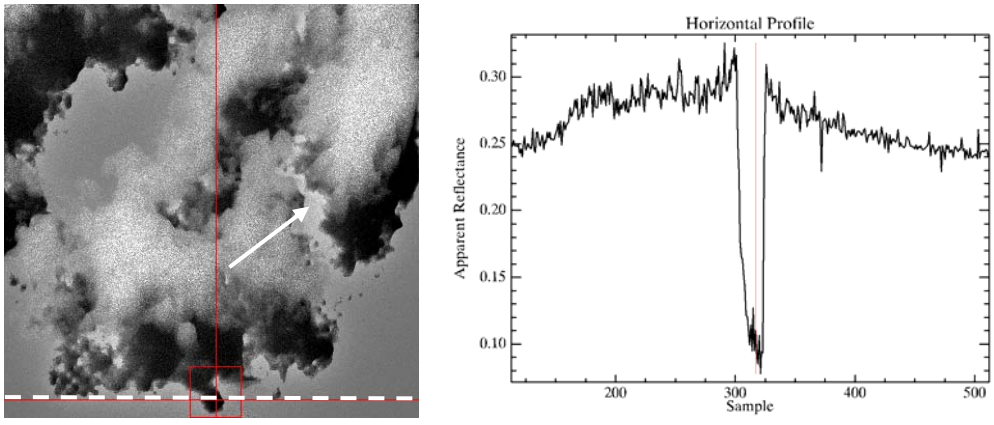

Fig. 5. Variation of illumination across a cloud shadow for the conditions of Fig. 2. The right-hand Fig. shows a slice of the image across the dashed line at left. The arrow indicates a region of significant cloud enhancement of surface illumination.

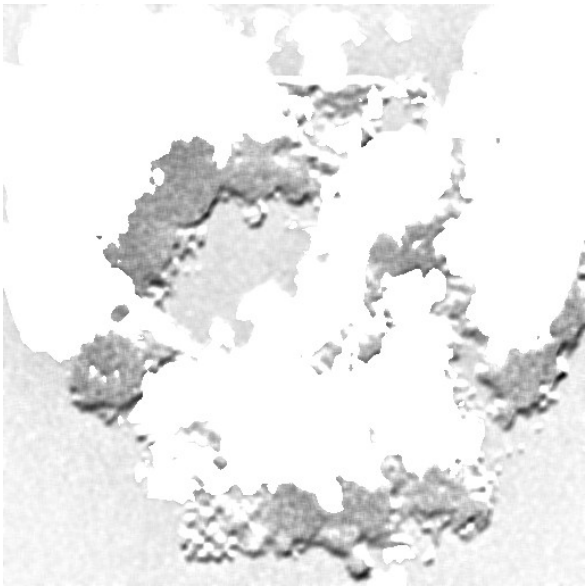

Fig. 6. Map of apparent atmospheric spherical albedo in the CFLOS areas of Fig. 2 (white=0, black=0.7).

A map of the atmospheric spherical albedo, S, at a wavelength of 1.0 μm was made by combining three MCScene images with surface reflectances, r, corresponding to 0, 0.25 and 1.0 via the equation

$$L = L_0 + a\rho/(1-\rho S) \tag{5}$$

where L designates radiance or (as in MCScene) apparent reflectance, L_0 designates the contribution from path scattering (solar photons that never hit the ground) and a is a constant proportional to the transmitted solar illumination, excluding reflections off the ground. Eq. (5) represents the standard hyperspectral radiation transport equation[7] for a horizontally uniform surface and atmosphere. The three images L yield three equations for Eq. (5) which were solved for S in the CFLOS areas of the scene. It should be noted that in applying this method to cloud-containing scenes, the results are not directly interpretable as an atmospheric reflectance, so they are referred to as "apparent" S values.

Apparent atmospheric spherical albedo values for the scene in Fig. 5 are shown in Fig. 6. In the sunlit areas, which appear as light gray, the S values are modest, around 0.05, with slightly higher values occurring near the center of the cloud field. Much higher values, averaging around 0.22, occur in shadowed regions. Since the cloud-reflected (trapped) downwelling radiation flux is expected to be similar in shadowed and sunlit regions, the difference in apparent S values is ascribed to the difference in total illumination. Even larger apparent S values, up to ~0.7, as well as some negative values (not shown) occur near the shadow edges; these are not presently understood. We estimate the "true" reflectance of the cloudy atmosphere to be around 0.1, in between the shadowed and sunlit apparent S values.

Simulation and analysis of a cloudy hyperspectral image

A demonstration of MCScene's HSI simulation capabilities with a cloud field was conducted by combining surface reflectance data from a HyMap sensor image with the nimbostratus cloud field, as illustrated in Fig. 7. The HyMap data of Davis, CA, were acquired by HyVista Corp. in a field experiment conducted by Spectral Sciences, Inc. and Kodak under a NASA-sponsored Small Business Innovative Research program.[14] The data were atmospherically corrected using the MODTRAN®-based FLAASH algorithm.[7,8] The resulting surface reflectances, which have been validated against ground truth reflectance tarps, were interpolated across opaque water band regions and georectified to a pixel size of 2.75 m using a registration map provided by HyVista. The surface reflectance image regridded to the MCScene pixels is shown in true color at left in Fig. 8. For the MCScene simulation, the viewing and solar geometries of Fig. 2 were used, which placed approximately half of the image in cloud shadow. The atmospheric parameters of the simulation are based on the MODTRAN® Subarctic Summer model with reduced atmospheric water vapor, the rural aerosol model and visibility of 50 km.

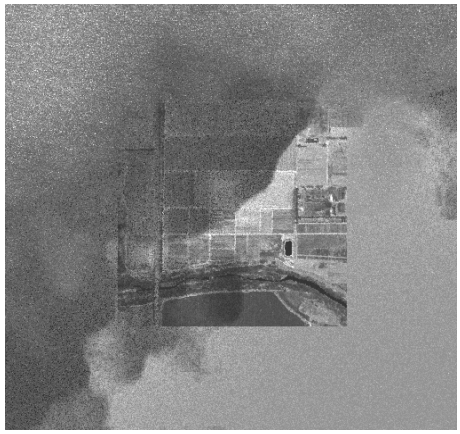

Fig. 7. Placement of the Davis, CA, hyperspectral scene in the MCScene cloud field simulation.

Fig. 8. Davis, CA hyperspectral scene simulations. At left, input surface reflectance; at center, MCScene apparent reflectance output; at right, the result after noise removal.

The center image in Fig. 8 shows the raw MCScene output at 200 photons/pixel. The photon statistical "noise" gives the image a speckled appearance. The right-hand image shows the much cleaner output obtained by applying the noise removal algorithm described in the Appendix. In this algorithm we used a 9x9 smoothing window and the left-hand image in Fig. 8 as the reference image for re-sharpening. Fig. 9 compares some example pixel spectra in the raw and noise-removed data cubes, and shows that the noise-removal has made the spectra much cleaner, revealing the true atmospheric absorption features.

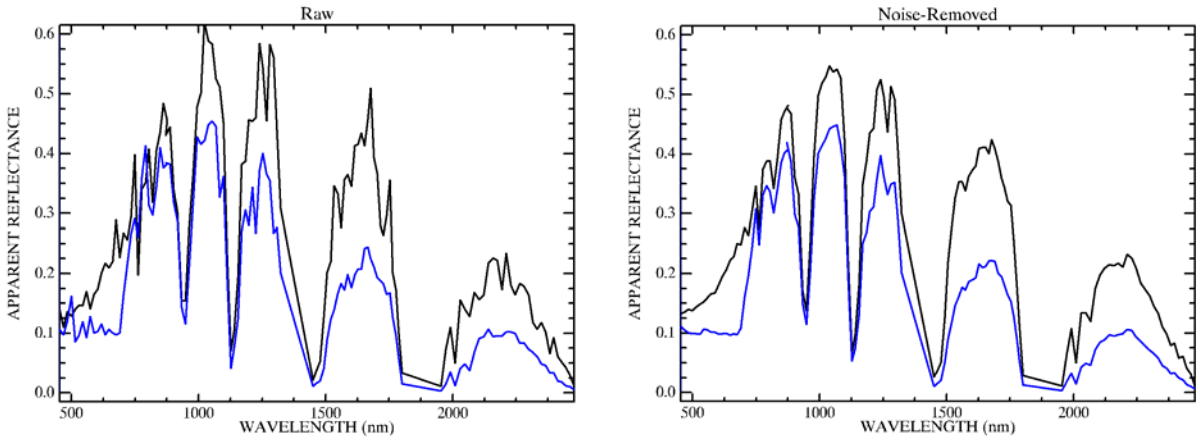

Fig. 9. Apparent reflectance spectra from the Davis, CA, hyperspectral scene simulation. At left, raw spectra of two pixels; at right, spectra of the same pixels after noise removal.

A useful indicator of the quality of a spectral image is its number of clutter-dominated (non-noisy) principal components, which is a measure of spectral information content. There are only five such principal components in the raw MCScene output but more than thirteen in the noise-removed output, comparable to the number in the original reflectance data.

The noise-removed MCScene-simulated image was analyzed by converting from apparent reflectance units to radiance units using the solar irradiance and then atmospherically correcting with FLAASH. In the FLAASH run, column water vapor was retrieved, while visibility was set to the input of 50 km. Some examples of the resulting reflectance spectra are shown in Fig. 10 along with the original inputs into MCScene. The results are very similar to the input spectra in the sunlit portion of the image, except for the addition of some noise and a slight reduction at the short wavelength end. A further reduction in noise was achieved by a principal components truncation, in which a principal components analysis of the simulated image was performed and the image reconstructed from the first twenty principal components.

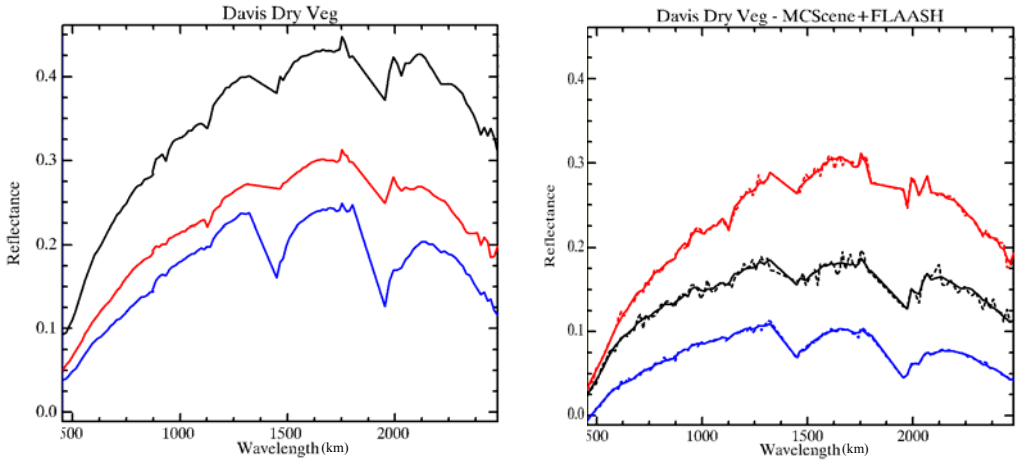

Fig. 10. Pixel reflectance spectra of dry vegetation input to MCScene (left) and output from MCScene after FLAASH processing (right). The thick solid curves at right have been processed with principal components truncation. The red curve denotes a sunlit pixel, while the black and blue curves denote shadowed pixels in the MCScene image.

Quantitative comparisons of the FLAASH-corrected MCScene image with the input reflectance are shown in the form of spectral ratios in Fig. 11. For the sunlit pixel the ratio is very close to 1 beyond ~600 nm, implying that the FLAASH atmospheric correction and MCScene forward simulation methods are highly consistent at these wavelengths. The reduction in the ratio at shorter wavelengths indicates that more atmospheric path radiance, from aerosol and/or Rayleigh scattering, is being removed by FLAASH than is being generated by MCScene. This discrepancy is much more pronounced in the cloud shadow, where there is decreased illumination of the atmospheric path. For the shadowed pixel, the ratio away from the short-wavelength end reflects the difference in illumination in the cloud shadow versus full sunlight. A more accurate estimate of the relative illumination in and out of cloud shadows is obtained by taking a ratio of reflectance differences between nearby pixels (Fig 11, rightmost plot), where the differencing cancels out the path radiance contribution. Here the illumination ratio decreases steadily from short to long wavelengths. Some water absorption features are also present.

The spectral dependence of the shadow-to-sunlit illumination ratio may reflect a number of sources, including radiation trapping (that is, the atmospheric spherical albedo effect) and illumination of the cloud shadow through the clear sky. The dependence may however be best explained by illumination diffusely transmitted through the cloud. The nimbostratus cloud extinction coefficient in MCScene, which derives from MODTRAN®, shows a slight increase (less than 10%) with wavelength over the 0.5-2.5 μm range of these data; this variation would however be magnified greatly by multiple scattering. We note that a study on cloud shadow removal[13] using real spectral imagery also observed decreased cloud shadow illumination, that is, increased cloud shadow depths, at infrared versus visible wavelengths. The water features in the illumination ratio appear to be of liquid water, and may derive from the cloud single scatter albedo, where such features are present at the level of a few percent. Finally, while the long paths of the multiply scattered photons also lead to increased absorption by atmospheric water vapor, this should not impact the retrieved surface reflectance, as it simply results in a compensatory increase in the FLAASH-retrieved column water vapor, by roughly 10%, in the shadows relative to the sunlit areas. This effect is also observed with real data.[15]

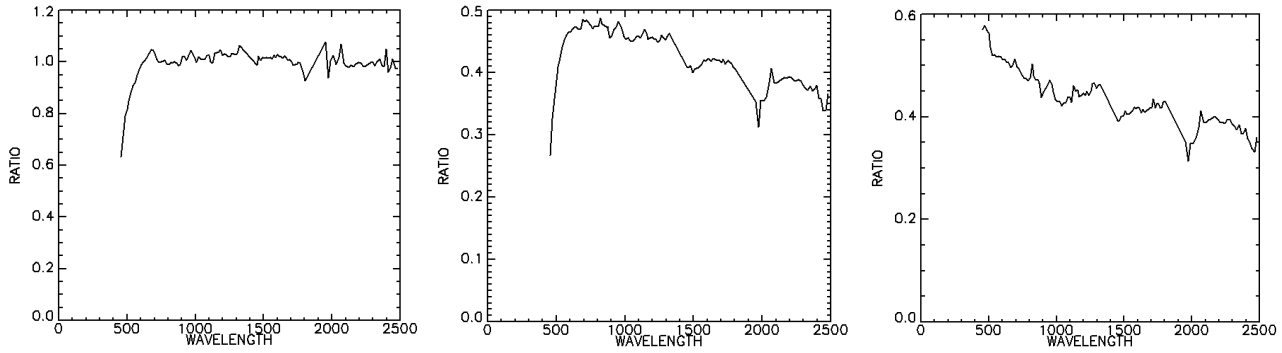

Fig. 11. Ratios of FLAASH reflectance retrievals to inputs into MCScene. From left to right, sunlit spectrum ratio, shadowed spectrum ratio and the ratio of shadowed spectrum differences, interpreted as the shadow-to-sunlit illumination ratio.

SUMMARY AND CONCLUSIONS

MCScene model simulations conducted with realistic cloud fields are shown to provide a useful tool for studying cloud obscuration, shadowing and illumination effects in spectral imagery in both nadir- and off-nadir (slant) viewing geometries. Calculations of LOS cloud obscuration were performed as a function of viewing angle, and were found to be accurately parameterized by a simple analytical model. The excellent agreement of this model with the simulations suggests that the model may be a useful planning tool for remote-sensing missions conducted with both space-based and airborne sensors. Both the analytical model and the MCScene simulations predict significant decreases in the CFLOS with increasing off-nadir viewing angle, together with an equivalent decrease in the sunlit fraction of the scene with increasing off-nadir solar angle. In applying these results to space-based sensors, the LOS angles should be measured with respect to the ground rather than the sensor to minimize effects of the Earth's curvature.

Analysis of simulated apparent reflectances revealed up to ~50% enhancement of full solar illumination by cloud scattering. Illumination levels in the cloud shadows were upward of 20% despite high cloud optical depths (up to 10). Some of this illumination is from sunlight scattered off the cloud tops and sides, while a significant part is also attributed to radiative trapping between the ground and the clouds, as described by an atmospheric spherical albedo.

A MCScene simulation of a hyperspectral scene with cloud shadows reproduces the key shadowing effects found in real data, and establishes a level of consistency between the MCScene model and the FLAASH atmospheric-correction algorithm. Slight reductions in illumination (deeper shadowing) are observed with increasing wavelength and in liquid water band regions. The former observation is consistent with a previous analysis of cloud shadows in real imagery.[13] The MCScene calculations also predict enhancement of FLAASH-retrieved column water vapor retrievals in cloud shadows, also in accord with observations.

ACKNOWLEDGEMENTS

The authors are grateful to Dr. A. Berk (Spectral Sciences, Inc.) and Dr. J. Roadcap (Air Force Research Laboratory) for critical technical reviews, Dr. R. Sundberg (Spectral Sciences, Inc.) for technical consultations and the Small Business Administration for funding under a Small Business Innovative Research Contract No. FA8718-05-C-0008.

REFERENCES

[1] Adler-Golden, S.M., L.S. Bernstein, M. W. Matthew, R.L. Sundberg and A.J. Ratkowski, "Atmospheric Compensation of Extreme Off-Nadir Hyperspectral Imagery from Hyperion," Proc. SPIE Vol. 6565, Algorithms and Technologies for Multispectral, Hyperspectral, and Ultraspectral Imagery XIII, Sylvia S. Shen and Paul E. Lewis, Eds., pp. 65651P (2007).

[2] Golemboski, J.J., "Analysis of Cloud-Free Line of Sight Probability Calculations," Air Force Institute of Technology, Wright-Patterson AFB, Master's Thesis, Report No. A926293 (March 2001).

[3] Lund, I. and Bertoni, E., "Some Comparisons between Probabilities of Cloud-Free Lines-of-Sight Estimated from Aircraft and from Sky Cover Observations," Air Force Geophysics Laboratory, Hanscom AFB, DTIC No. ADC021847 (February 1980).
[4] Richtsmeier, S.C., A. Berk, S.M. Adler-Golden and L.S. Bernstein, "A 3D Radiative-Transfer Hyperspectral Image Simulator for Algorithm Validation," Proceedings of ISSSR 2001, Quebec City, Canada (June 2001).
[5] Richtsmeier, S.C. and R.L. Sundberg, "Hyperspectral Scene Simulation in the Ultraviolet through Longwavelength Infrared: MCScene Users Manual," SSI-TR-446, Spectral Sciences, Inc., Burlington MA (February 2008).
[6] Cianciolo, M.E. and M.E. Raffensberger, "Atmospheric Scene Simulation Modeling and Visualization: Cloud Scene Simulation Model User's Guide," TASC Report No. TIM-07169-2, prepared for Phillips Laboratory Geophysics Directorate and Electronic Systems Center, Hanscom AFB, MA under Contract No. F19628-93-C-0203 (April 1996).
[7] Adler-Golden, S.M., M.W. Matthew, L.S. Bernstein, R.Y. Levine, A. Berk, S.C. Richtsmeier, P.K. Acharya, G.P. Anderson, G. Felde, J. Gardner, M. Hoke, L.S. Jeong, B. Pukall, J. Mello, A. Ratkowski and H.-H. Burke, "Atmospheric Correction for Short-wavelength Spectral Imagery based on MODTRAN4," Proc. SPIE Vol. 3753, Imaging Spectrometry V, pp. 61-69 (1999).
[8] Matthew, M.W., S.M. Adler-Golden, A. Berk, G. Felde, G.P. Anderson, D. Gorodetzky, S. Paswaters, and M. Shippert, "Atmospheric Correction of Spectral Imagery: Evaluation of the FLAASH Algorithm with AVIRIS Data," Proc. SPIE Vol. 5093, Algorithms and Technologies for Multispectral, Hyperspectral, and Ultraspectral Imagery IX, Sylvia S. Shen and Paul E. Lewis, Eds., pp. 474-482 (2003).
[9] Tanré, D., P.Y. Deschamps, P. Duhaut and M. Herman, "Adjacency Effect Produced by the Atmospheric Scattering in Thematic Mapper Data," J. Geophys. Res. 92, 12000 (1987).
[10] Walthall, C.L., J.M. Norman, J.M. Wes, G. Campbell and B.L. Blad, "Simple Equation to Approximate the Bidirectional Reflectance from Vegetation Canopies and Bare Soil Surfaces," Appl. Optics 24:383-387 (1985).
[11] Berk, A., L.S. Bernstein and D.C. Robertson, "MODTRAN: A Moderate-Resolution Model for LOWTRAN 7," GL-TR-89-0122, Geophysics Directorate, Phillips Laboratory, Hanscom AFB, MA 01731 (April 1989) ADA214337.
[12] Adler-Golden, S.M., R.Y. Levine, M.W. Matthew, S.C. Richtsmeier, L.S. Bernstein, J.H. Gruninger, G. Felde, M. Hoke, G.P. Anderson and A. Ratkowski, "Shadow-Insensitive Material Detection/Classification with Atmospherically Corrected Hyperspectral Imagery," Proc. SPIE Vol. 4381, Algorithms for Multispectral, Hyperspectral, and Ultraspectral Imagery VII, Sylvia S. Shen and Michael R. Descour, Eds., pp. 460-469 (2001).
[13] Adler-Golden, S.M., M.W. Matthew, G.P. Anderson, G.W. Felde and J.A. Gardner, "An Algorithm for De-Shadowing Spectral Imagery," Presented at the AVIRIS Earth Sciences and Applications Workshop, NASA Jet Propulsion Laboratory (2002).
[14] Rochford, P.A., P.K. Acharya, S.M. Adler-Golden, A. Berk, L.S. Bernstein, M.W. Matthew, S.C. Richtsmeier, S. Gulick, Jr. and J. Slusser, "Validation and Refinement of Hyperspectral/Multispectral Atmospheric Compensation Using Shadowband Radiometers," IEEE Trans. Geosci. Remote Sens., 43, 2898-2907 (2005).
[15] Borel, C.C., P.V. Villeneuve, W.B. Clodius, J.J. Szymanski and A.B. Davis, "Practical Atmospheric Correction Algorithms for a Multi-Spectral Sensor from the Visible through the Thermal Spectral Regions," Proc. SPIE, Vol. 3717, Algorithms for Multispectral and Hyperspectral Imagery V, Sylvia S. Shen and Michael R. Descour, Eds., pp 158-168 (1999).
[16] Hill, J., C. Diemer, O. Stöver and Th. Udelhoven, "A local correlation approach for the fusion of remote sensing data with different spatial resolutions in forestry applications," International Archives of Photogrammetry and Remote Sensing, Vol. 32, Part 7-4-3 W6, Valladolid, Spain, 3-4 June (1999).
[17] Tom, V.T. and M.J. Carlotto, "Adaptive least-squares technique for multi-band image enhancement," Proc. ICASSP International Conference on Acoustics, Speech and Signal Processing, Tampa, Florida, 26-29 March, pp. 704-707 (1985).

APPENDIX: NOISE REMOVAL METHOD FOR CLOUD SCENE SIMULATIONS

The SSI MCScene code enables simulation of hyperspectral or multispectral data cubes with arbitrary atmospheric conditions, including an overlaid cloud field. Its main drawback for cloudy scenes is the long computation times (an order of magnitude longer than in cloud-free scenes) required to propagate the Monte Carlo "photons". . Assembly of a cloudy synthetic data cube with good signal-to-noise ratios may therefore require days to weeks of computation time, even on a multiprocessor cluster. Herein we describe a method that improves the fidelity of noisy (low photon count) simulations with the aid of a "reference" cube, which may consist of a high-fidelity clear scene or the reflectance input

cube. While the method does introduce some artifacts, described below, overall it provides a dramatic improvement in fidelity, corresponding to a computational savings of an order of magnitude or more, when starting from a noisy (~100 photons/pixel) cloud-containing data cube.

The noise-removal method derives from a local correlation-based image-sharpening algorithm.[16,17] Essentially, the cloud-containing synthetic cube is spatially smoothed to reduce noise, and it is then sharpened by adding surface detail from the reference cube. Since cloud edges do not appear in the reference cube, their spatial detail is not restored, so the clouds are somewhat blurred in the output image. While this effect is a source of error, it tends to enhance rather than degrade the subjective appearance of the MCScene image, perhaps because the cloud edges in the Cloud Scene Simulation Model used by MCScene appear to be unrealistically sharp.

The working equation is

$$I_{noise\ removed} = \langle I \rangle + m\left(I_r - \langle I_r \rangle\right) \tag{A1}$$

where I is the MCScene image for a given spectral channel, $\langle I \rangle$ is the corresponding smoothed image, the subscript "r" refers to the reference image and m is a pixel-specific correlation coefficient obtained from a local linear regression analysis. Essentially, m determines the amount of surface detail, defined by the $(I_r - \langle I_r \rangle)$ factor, that is restored in each pixel. The smoothing is efficiently performed in IDL code with a square window of user-selected size, typically between 5x5 and 11x11 pixels. The regression analysis is performed within this same window, leading to

$$m = \frac{\langle I_r I \rangle - \langle I_r \rangle \langle I \rangle}{\langle I_r^2 \rangle - \langle I_r \rangle^2} \tag{A2}$$

The qualitative success of this method in a hyperspectral application is seen in Fig. 8. A quantitative study was performed using a RGB reference scene generated by MCScene with a clear sky using 10,000 photons/pixel. A cumulus cloud field was added and three new scenes were generated: a very noisy one using 100 photons/pixel and two less-noisy ones using 1000 and 10,000 photons/pixel. The noise-removal method was employed with a 7x7-pixel window on the noisiest two scenes (100 photons/pixel and 1000 photons/pixel). The overall improvement in fidelity due to noise removal is seen in the Fig. A1 correlation plots. The noise-removed 100 photons/pixel image has a slightly tighter correlation with the ground truth than does the 1000 photons/pixel image, which takes ten times longer to compute.

Computations of RMS differences with respect to the "ground truth" (10,000 photons/pixel) image provide additional quantitative measures of performance. Noise removal yields an approximately fourfold improvement in RMS accuracy at 100 photons/pixel and an approximately twofold improvement at 1000 photons/pixel. The noise removal is more effective than increasing the number of photons from 100 to 1000 per pixel, which would be expected to improve accuracy, at best, by the expected $10^{1/2}$ (=3.16) statistical factor. Not surprisingly, with noisier images larger smoothing windows yield the best accuracy. The best overall window size in these simulations is approximately 7x7 pixels.

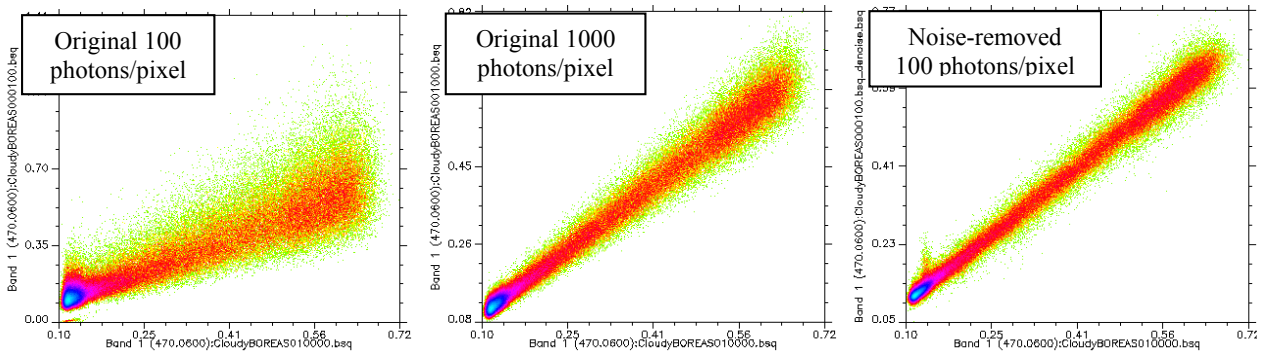

Fig. A1. Correlations of blue (~450 nm) channel values (y-axis) versus "ground truth" (10,000 photons/pixel) values (x-axis), in order of increasing image fidelity from left to right. Units are apparent reflectance.